An Automatic Coil Design Method With Modified AC Resistance Evaluation for Achieving Maximum Coil–Coil Efficiency in WPT Systems

Guo Wei, Xiulang Jin, Chao Wang, Jing Feng, Chunbo Zhu, *Member, IEEE*, and Milyaev Igor Matveevich

***Abstract*—In wireless power transfer systems, coil design has a great impact on coil–coil efficiency. This article analyzes the relationship between coil–coil efficiency and design parameters (three geometric parameters of coupling coils and working frequency) under typical constraints, and the function between optimal working frequency and geometric parameters is derived. Hence, the solution space of design parameters is reduced from four dimensions (geometric parameters of the coil and frequency) to three dimensions (geometric parameters), and particle swarm optimization (PSO) algorithm is applied to solve it. Moreover, a modified ac resistance evaluation method is proposed, in which conductive resistance is calculated with a frequency-dependent formula and proximity-effect resistance is calculated with a modified analytical method. Experimental results show that the modified method is precise for coils wound closely or sparsely. It is highlighted that extra finite element analysis software is not needed due to the modified calculation method of ac resistance, which makes the design process automatic and faster. Finally, a practical example is given, and two systems are designed with the PSO-based method and a conventional method, respectively. The coil–coil efficiency of the PSO-based method and the conventional method is 95.6% and 94.0%, respectively.**

***Index Terms*—AC resistance evaluation, automatic coil design, coil–coil efficiency, particle swarm optimization (PSO), wireless power transfer (WPT).**

I. Introduction

WIRELESS power transfer (WPT) technology has been applied in many fields, such as electric vehicles [1], biomedical implants [2], and data transmission [3]. Power transfer efficiency is one of the key factors to evaluate a WPT system. The transfer efficiency is mainly determined by inverter efficiency and coil–coil efficiency, and this article focuses on the latter, which can be optimized by coupling coils design.

So far, many efforts have been made for the high-efficiency coupling coils design under various design constraints. In this article, the varying load conditions (such as charging a battery) are not considered. Consequently, the design constraints can be classified into four types according to the working frequency and the load resistance.

1) The load and the working frequency are allowed to be chosen in a wide range [4], [5].
2) The load can be chosen freely while the working frequency is given ahead, such as 85 kHz or 6.78 MHz [6].
3) The load is given ahead while the working frequency can be chosen freely [7], [8].
4) The load and the working frequency are given ahead [9], [10].

The design metrics of type 1) and type 2) is the quality factor (Q) or kQ (coupling coefficient multiplies Q) of coils, because the coil–coil efficiency can be expressed as a function related only to kQ when the load resistance can be matched freely. Consequently, a higher coil–coil efficiency can be achieved under a higher Q or kQ by adjusting the load resistance [4]. A type of coil with non-uniform wire diameter is presented in [11], and the Q of the improved coil is 1.21 times higher than that of the conventional coil. Obviously, it is not suitable for coils wound by Litz-wire due to constant wire diameter. Moreover, a set of design formulas have been derived to develop new design procedures, then coil parameters including number of turns, outer and inner radii can be optimized one by one with respect to kQ [5], [12].

However, for constraints type 3) or type 4), in which load resistance is prefixed, the coil–coil efficiency cannot be expressed as a function related only to kQ. Thus, Q or kQ is not the only key factor of coil–coil efficiency. For example, the prefixed parameters in [13] are coil shape and dimensions, air gap, maximum operating frequency, primary voltage, and equivalent resistance of the load. Consequently, a new design factor depending on both Q and the frequency is obtained through analysis. The work in [14] also presents a new figure-of-merit to balance the optimal efficiency and the maximum output power. The coil design method in this article is based on constraints type 3), which can be applied for heating appliances, such as rice cooker or hot water pot. A simple design procedure for

Manuscript received June 14, 2019; revised August 22, 2019 and October 13, 2019; accepted October 31, 2019. Date of publication November 7, 2019; date of current version February 20, 2020. This work was supported by the National Natural Science Foundation of China under Grant 51577041 and 51811530102. Recommended for publication by Associate Editor J. M. R. Davila. *(Corresponding author: Guo Wei.)*

G. Wei, X. Jin, C. Wang, J. Feng, and C. Zhu are with the School of Electrical Engineering and Automation, Harbin Institute of Technology, Harbin 15001, China (e-mail: hitweiguo@hit.edu.cn; jinxiulang1994@foxmail.com; chaowang@stu.hit.edu.cn; fengjing419htu@163.com; zhuchunbo@hit.edu.cn).

M. I. Matveevich is with the Baikov Institute of Metallurgy and Material Science, Russian Academy of Sciences, Moscow 119991, Russia (e-mail: imilyacv@mail.ru).

Color versions of one or more of the figures in this article are available online at http://ieeexplore.ieee.org.

Digital Object Identifier 10.1109/TPEL.2019.2952120

this constraints type is presented in [8], in which the innermost radius is set to be half of the outermost radius to achieve the maximum coupling coefficient and minimize ac resistance, and the inductance is determined via the coupling coefficient, load resistance, and maximum working frequency. Finally, the number of turns is calculated by empirical formulas to satisfy the inductance. The method is simple and high coil–coil efficiency can be obtained, whereas the accuracy is not enough, because the inductance and ac resistance of coils are calculated by empirical formulas. Therefore, the highest coil–coil efficiency is not guaranteed.

Multi-parameter optimization can be used to solve the optimal design parameters. First, the efficiency analysis is conducted to get the optimization target, then the exhaustive search algorithm is usually applied to obtain the optimal design parameters [5], [9], [12]–[14]. Nevertheless, the computation will be huge when the number of optimization parameters is three or more. Compared with the exhaustive search algorithm, intelligent optimization algorithms such as genetic algorithm [15] and Tabu search algorithm [10] require much smaller computation. Moreover, the particle swarm optimization (PSO) algorithm can obtain more precise result due to the flexible search step [16].

Generally, the optimization loop of intelligent algorithms contains two parts: the fitness value calculation and the parameter update. The former includes the calculation of self-inductance, mutual inductance, and ac resistance of coils. The existing calculation methods can be classified into three categories: empirical formulas [5], [13], [15], finite element analysis (FEA) [10], [17]–[19], and analytical methods [9], [20]. The first kind requires minimum computation, but the error may be larger. FEA software can analyze the original shape and dimension of a coil without simplification. However, the twisting structure of Litz-wire cannot be simulated, which can bring errors when calculating ac resistance. What is more, the optimization process will be time-consuming and non-automatic. Compared with the two types of methods above, analytical methods can be used to balance the precision and computation load. Nevertheless, the existing methods of ac resistance are mainly for coils wound closely, not sparsely. Moreover, the current distribution is always treated as constant among different strands of high-frequency Litz-wire, which is actually not true due to the imperfect twisting of Litz-wire [21].

The purpose of this work is to present a PSO-based coil design method with precise ac resistance evaluation. Series–series (S-S) compensation topology is studied as an example. In practice, load resistance, frequency design scope, output power, air gap, and radius limitation are given. With the aforementioned constraints, the relationship between coil–coil efficiency and design parameters (geometric parameters of coils and working frequency) is analyzed, and the optimal working frequency related to geometric parameters is obtained. Then, the coil design problem is transformed into a three-objective (turn-spacing, the number of turns and the outermost radius of coils) optimization problem. Aiming at maximum coil–coil efficiency, the PSO is employed to solve the optimization problem. It is highlighted that the design method can be implemented automatically due to the analytical calculation methods of mutual inductance and ac resistance. A frequency-dependent fitting formula and a modified analytical method are proposed for the calculation of conductive resistance and proximity-effect resistance, respectively. As a result, the modified calculation method of ac resistance is precise for coils with various turn-spacing in a wide range of frequencies.

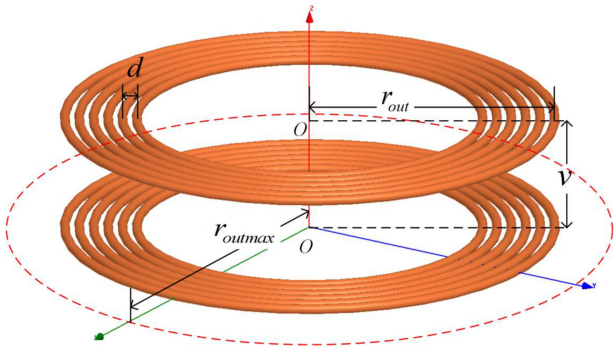

Fig. 1. Concentric-turns model of coupling coils.

The contribution of this article is as follows.

1) An improved analytical calculation method is proposed for z resistance, which is precise for Litz-wire coils and promotes the automatic design process of coils;
2) The function between the optimal frequency and geometric parameters of coils is derived under special constraints. Consequently, the solution space is reduced from four dimensions to three dimensions, which reduces the optimization complexity and the amount of calculation.
3) An automatic PSO-based coil design method is constructed for solving the optimal design parameters corresponding to the maximum coil–coil efficiency.

The rest of this article is organized as follows. In Section II, the geometric parameters of coils and the modified calculation method of ac resistance are introduced. Section III presents the relationship between coil–coil efficiency and design parameters with S-S topology under typical design constraints, and the optimal frequency is derived. Furthermore, the PSO algorithm is applied in a design example to explain the application of the proposed method. In Section IV, an experimental prototype is built to validate the theoretical results. Finally, Section V concludes this article.

II. Parameters of Coupling Coils and Modified Calculation Method of AC Resistance

A. Geometric Parameters of Coupling Coils

In this study, the planar spiral coils wound by Litz-wire is used. For the planar spiral coil, the concentric-turns equivalent configuration, as shown in Fig. 1, is applied when the space between two adjacent turns is much smaller than the radius of the turn [17]. The equivalence is applied for the calculation of the ac resistance and the mutual inductance. The parameter d represents turn-spacing of the coil, which is the distance between the centers of adjacent turns, and the coil is wound with uniform turn-spacing. v is the gap between coupling coils. $r_{\rm out}$ and

r_{outmax} are the radius of the outermost turn and its design limit, respectively. Therefore, each coil can be uniquely characterized by parameters d, r_{out}, and the number of turns N_t.

Generally, high-frequency resistance of a coil is comprised of the conductive resistance and the proximity resistance. Though Litz-wire can restrain the skin effect caused by eddy currents, the proximity-effect resistance of multiturn coils cannot be ignored. Most researchers preferred to wound coils closely to get larger inductance, which has a positive effect on coil–coil efficiency. However, the proximity-effect resistance will be increased as the turn-spacing decreases, which will result in a negative effect on efficiency. Therefore, the coil–coil efficiency can be optimized by exploring the optimum turn-spacing.

In this article, an optimization algorithm including analytical calculation methods of the ac resistance and the mutual inductance is used to obtain the optimal *d* and other geometric parameters of coils to achieve maximum coil–coil efficiency under design constraints. The following parts introduce the calculation methods of ac resistance and mutual inductance.

B. Modified Calculation Method of AC Resistance

The ac resistance of a Litz-wire coil can be expressed as follows [4], [20]:

$$R_0 = R_{\text{cond}} + R_{\text{prox}} = \sum_{i=1}^{N_t} (R_{\text{cond\_}i} + R_{\text{prox\_}i}) \tag{1}$$

where R_{cond} represents the dc conductive resistance and R_{prox} represents the proximity-effect resistance; $R_{\text{cond\_}i}$ and $R_{\text{prox\_i}}$ are conductive resistance and proximity-effect resistance of the *i*th turn, respectively. It should be noted that the skin effect can be ignored when r_s is far lower than ρ_{skin} [4], where r_s and ρ_{skin} denote the radius and the skin depth of strands, respectively. ρ_{skin} can be calculated as $\sqrt{2/\mu\sigma\omega}$, where σ and μ are conductivity and permeability of copper, respectively, and ω denotes the current frequency. The calculation formulas of $R_{\text{cond\_}i}$ and $R_{\text{prox\_}i}$ are

$$R_{\text{cond\_}i} = 2r_i/(n_0 r_s^2 \sigma) \tag{2}$$

$$R_{\text{prox\_}i} \approx \frac{n_0 \pi^2 \mu^2 \sigma r_s^4 r_i H_{avg}^2(i)}{2I^2} \omega^2 \tag{3}$$

where r_i and n_0 are the radius of the *i*th turn and the number of strings, respectively. $H_{\text{avg}}^2(i)$ is the average squared magnetic field strength over the cross section of the *i*th turn, and it is worth mentioning that $H_{\text{avg}}^2(i)$ is constant along the *i*th turn due to the symmetrical structure of the coil. *I* denotes the rms amplitude of the current flowing through the coil.

1) Modified Calculation Method of Proximity-Effect Resistance: According to (3), the major work is to calculate $H_{\text{avg}}^2(i)$. The field strength throughout the cross section of the *i*th turn is the superposition of the field strength, which is generated by the *i*th turn and the rest of the turns. $H_{\text{avg}}^2(i)$ can be expressed as follows [20]:

$$H_{\text{avg}}^2(i) = H_{\text{avg\_self}}^2(i) + H_{\text{avg\_else}}^2(i) + H_{\text{cross}}^2(i) \tag{4}$$

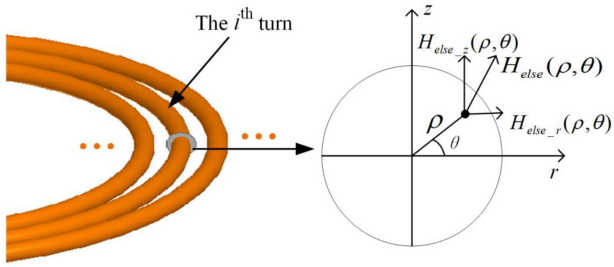

Fig. 2. Magnetic field vector over the cross section of the *i*th turn, and the components along the *r*-direction and *z*-direction.

where $H_{\text{avg\_self}}^2(i)$ is the average squared field strength over the cross section generated by the *i*th turn itself, and $H_{\text{avg\_else}}^2(i)$ is the average squared field strength over the cross section created by the rest of turns. $H_{\text{cross}}^2(i)$ is the cross field strength due to the magnetic field interaction between $H_{\text{avg\_self}}^2(i)$ and $H_{\text{avg\_else}}^2(i)$, which can be given by

$$H_{\text{cross}}^2(i) = \frac{2}{\pi r_c^2} \int_0^{2\pi} \int_0^{r_c} H_{\text{self}}(\rho)(H_{\text{else\_}r}(\rho,\theta)\sin\theta + H_{\text{else\_}z}(\rho,\theta)\cos\theta) d\rho d\theta \tag{5}$$

where $H_{\text{self}}(\rho)$ is the field strength at radius of ρ generated by the *i*th turn. $H_{\text{else\_}r}(\rho,\theta)$ and $H_{\text{else\_}z}(\rho,\theta)$ are, respectively, the components of $H_{\text{else}}(\rho,\theta)$ in two orthogonal directions, as shown in Fig. 2, where $H_{\text{else}}(\rho,\theta)$ is the field strength of point (ρ,θ) generated by the rest of the turns.

Acero *et al*. [20] assume that the field strength $H_{\text{else}}(\rho,\theta)$ is constant over the cross section, which means that $H_{\text{else\_}r}(\rho,\theta)$ and $H_{\text{else\_}z}(\rho,\theta)$ are irrelevant to ρ or θ. Then, according to (5), $H_{\text{cross}}^2(i) = 0$, and one may get

$$H_{\text{avg}}^2(i) = H_{\text{avg\_self}}^2(i) + H_{\text{avg\_else}}^2(i). \tag{6}$$

Based on the above analysis, $H_{\text{avg}}^2(i)$ is merely related to $H_{\text{avg\_self}}^2(i)$ and $H_{\text{avg\_else}}^2(i)$ and the work of analyzing the interactions magnetic field can be omitted. However, $H_{\text{else\_r}}(\rho,\theta)$ and $H_{\text{else\_}z}(\rho,\theta)$ are not identical according to formulas (28) and (31) in [20]. Thus, it is appropriate to use (6) to calculate $H_{\text{avg}}^2(i)$ when the experimental coil satisfies

$$H_{\text{cross}}^2(i) \ll H_{\text{avg\_self}}^2(i) + H_{\text{avg\_else}}^2(i). \tag{7}$$

For coils that cannot meet (7), great errors tend to be generated when substituting (4) with (6). To address this problem, the superposition of the field strength generated by all turns is analyzed to calculate $H_{\text{avg}}^2(i)$ in this article. In the following, the average squared field strength of the *i*th turn is analyzed as an example.

The cross section of the *i*th turn is put in polar coordinates, as illustrated in Fig. 3. $H(\rho,\theta_1)$ is the superposition of the field strength created by all turns at (ρ,θ_1), then the average squared field strength can be expressed as follows:

$$H_{\text{avg}}^2(i) = \frac{1}{\pi r_c^2} \int_0^{2\pi} \int_0^{r_c} H^2(\rho,\theta)\rho d\rho d\theta. \tag{8}$$

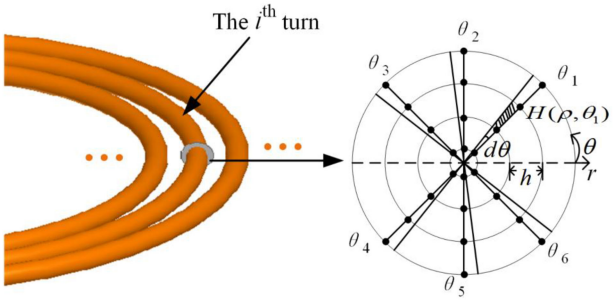

Fig. 3. Cross section of the *i*th turn and sample points on it.

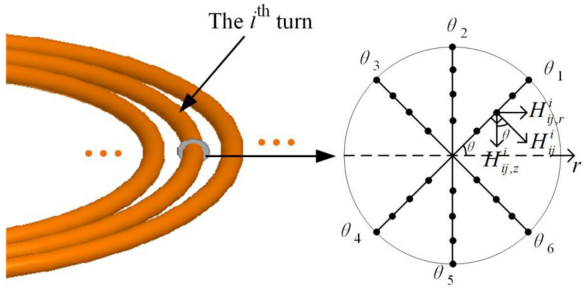

Fig. 4. Field strength over the cross section generated by the *i*th turn itself.

It is difficult to use the double-integral tool to calculate (8) because $H(\rho,\theta)$ contains a lot of integrals. In this work, a numerical integration method is proposed to calculate $H^2_{\text{avg}}(i)$. First, a multi-point average method is used to estimate the integration of variable θ. The integral interval of θ is $[0, 2\pi]$. Eight equidistant samples within $[0, 2\pi]$ are chosen to balance approximation accuracy and computing load. However, the calculation result of $H(\rho,\theta)$ is not convergent when θ is equal to 0 or π, which will be explained in the following analysis. Therefore, six sample points θ_i are chosen as $\pi/4$, $\pi/2$, $3\pi/4$, $5\pi/4$, $3\pi/2$, and $7\pi/4$, respectively. Consequently, the integral part of (8) can be estimated as follows:

$$\int_0^{2\pi}\int_0^{r_c} H^2(\rho,\theta)\rho d\rho d\theta \approx \frac{\sum_{m=1}^{6}\int_0^{r_c} H^2(\rho,\theta_m)\rho d\rho}{6}\cdot 2\pi. \tag{9}$$

For integrals in (9), equidistant points estimation is not suitable because $H^2(\rho,\theta_m)\rho$ varies along $(0, r_c)$ apparently. Therefore, four-notes Newton–Cotes integration formula is applied and can be expressed as follows:

$$\int_0^{r_c} H^2(\rho,\theta_m)d\rho \approx Ah\sum_{n=0}^{3} W_n H^2(\rho_n,\theta_m) \tag{10}$$

where $A = 3/8$, W_n(for n = 1, 2, 3, 4) are 1, 3, 3, and 1, respectively. $r_c/8$ and r_c are chosen to be the first and last sample points, respectively, and thus, the integral step size is $h = 7r_c/24$. Another two sample points are $5r_c/12$ and $17r_c/24$. Finally, $H^2_{\text{avg}}(i)$ can be calculated according to (8)–(10) as follows:

$$H^2_{\text{avg}}(i) \approx \frac{Ah\sum_{m=1}^{6}\sum_{n=0}^{3} W_n H^2(\rho_n,\theta_m)\rho_n}{3r_c^2}. \tag{11}$$

The following part explains how to calculate $H(\rho_n,\theta_m)$. For convenience, the field strength of the *j*th black points in Fig. 3 is denoted as $H_{ij}(j = 1, 2, \ldots, 24)$, then

$$H^2_{ij} = H^2_{ij,r} + H^2_{ij,z} \tag{12}$$

where $H_{ij,r}$ and $H_{ij,z}$ are, respectively, the components of H_{ij} in the radius direction and in the vertical direction of the plane on which the coil is placed. The directions are depicted in Fig. 2. Furthermore

$$H_{ij,r} = \sum_{p=1}^{N_t} H^p_{ij,r}, H_{ij,z} = \sum_{p=1}^{N_t} H^p_{ij,z} \tag{13}$$

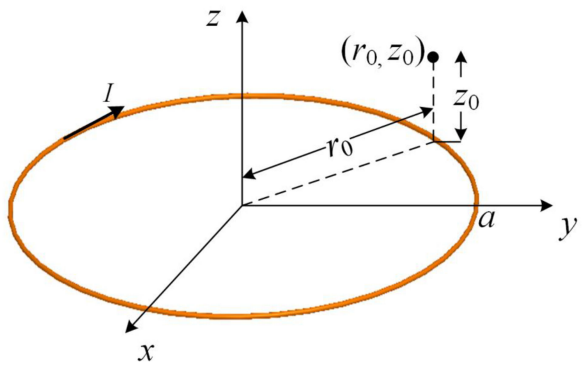

Fig. 5. Axis and circular filamentary current model.

where $H^p_{ij,r}$ and $H^p_{ij,z}$ are the two components of the field strength imposed on the *j*th point generated by the *p*th turn.

When calculating the field strength on the *j*th point generated by the *i*th turn itself, i.e., $H^i_{ij,r}$ and $H^i_{ij,z}$, as shown in Fig. 4, the Litz-wire can be viewed as the solid wire and Ampere's law is applied [20], and the formulas are as follows:

$$H^i_{ij} = B/\mu_0 = (1/2\pi\rho)\cdot(I\rho^2/r_c^2) = I\rho/2\pi r_c^2 \tag{14}$$

$$H^i_{ij,r} = H^i_{ij}\sin\theta\ ,\ H^i_{ij,z} = H^i_{ij}\ \cos\theta \tag{15}$$

where ρ and B are respectively the radius of the sample point and the magnetic flux density.

The following task is to calculate $H^p_{ij,r}(p \neq i)$ and $H^p_{ij,z}(p \neq i)$. Generally, Litz-wire is comprised of hundreds of twisted strands. It is hard to analyze the field strength generated by each strand individually. Thus, the Litz-wire is taken as the solid wire when the field strength generated by the *p*th turn is analyzed. Fig. 5 shows the axis and circular filamentary current model, and the field strength at point (r_0, z_0) generated by a circular filamentary current can be calculated by [20]

$$\begin{aligned} H_z(r_0,z_0) &= \frac{I}{2}a\int_0^{\infty} xe^{-x|z_0|}J_0(xr_0)J_1(xa)dx \\ H_r(r_0,z_0) &= \frac{I}{2}a\int_0^{\infty} xe^{-x|z_0|}J_1(xr_0)J_1(xa)dx \end{aligned} \tag{16}$$

where a is the radius of the filamentary coil and $J_0(x)$, $J_1(x)$ are Bessel functions. It can be easily proved that formulas in (16) are not convergent when $z_0 = 0$. Therefore, sample points of θ in (9) cannot be 0 or π.

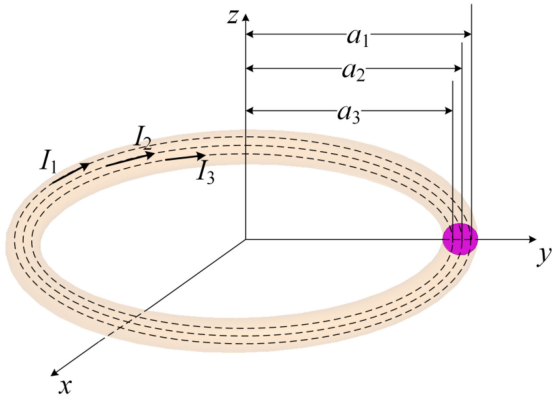

Fig. 6. Equivalent filamentary currents of the current flowing through the *p*th turn.

There exist countless filamentary currents flowing through the cross section of the equivalent solid wire. In this article, three filamentary currents are chosen to estimate the field strength generated by the *p*th turn. Though more than three filamentary currents can be chosen, the calculation result is almost the same as that for three or more currents. In Fig. 6, circular filamentary currents I_1, I_2, and I_3 are on the plane of the *p*th turn. I_1, I_2, and I_3 are identical with the current flowing through the Litz-wire coil. The radii of those filamentary currents are $a_1 = r_p + r_c/2$, $a_2 = r_p$, and $a_3 = r_p - r_c/2$, respectively.

Then $H_{ij,r}^{p}$ and $H_{ij,z}^{p}$ can be approximately calculated as follows:

$$H_{ij,r}^{p} \approx \frac{1}{3}(H_{ij,r}^{p_1} + H_{ij,r}^{p_2} + H_{ij,r}^{p_3})$$
$$H_{ij,z}^{p} \approx \frac{1}{3}(H_{ij,z}^{p_1} + H_{ij,z}^{p_2} + H_{ij,z}^{p_3}) \tag{17}$$

where $H_{ij,r}^{p_k}$ and $H_{ij,z}^{p_k}$ are the two components of the field strength imposed on the *j*th point created by filamentary current I_k (for $k = 1, 2, 3$). $H_{ij,r}^{p_k}$ and $H_{ij,z}^{p_k}$ can be calculated based on (16).

In this way, H_{ij} can be calculated by (12)–(17), then $H_{\text{avg}}^2(i)$ and $R_{\text{prox\_}i}$ can be obtained through (11) and (3).

FEA software has been usually used to calculate the magnetic field [17], [19]. However, there are several disadvantages of this technique. First, Litz-wire is treated as solid wire in FEA software, therefore the calculation results are the same for Litz-wires with equal radius but different twisting schemes, which does not accord with the practical results. In the next paragraph, a coefficient relates to Litz-wire type is proposed to reflect the difference. Second, the process of simulation is time-consuming, especially for the PSO algorithm. Third, the optimization process cannot be automatic when FEA software is required.

The calculation error of the modified method mainly comes from the calculations of $H_{ij,r}^{p}(p \neq i)$ and $H_{ij,z}^{p}(p \neq i)$. First, (16) is based on concentric-turns model while the real structure of coupling coils is a spiral shape. If the turn-spacing is much smaller than the radius of each turn, the relative error between equivalent model and real structure can be treated as irrelevant to the dimensions of coil. Second, (11) and (17) are used to estimate the field distribution over the cross section of the Litz-wire and the field strength created by the current flowing through the Litz-wire, respectively, which can bring approximation errors. The approximation errors are mainly determined by Litz-wire type and almost irrelevant to the dimensions of coils. Therefore, a correction factor k_{else} is introduced to modify the theoretical result. The modified field strength imposed on the *j*th point can be expressed as follows:

$$H'_{ij,r} \approx H_{ij,r}^{i} + k_{\text{else}} \sum_{p=1, p\neq i}^{N_t} H_{ij,r}^{p} \tag{18}$$

$$H'_{ij,z} \approx H_{ij,z}^{i} + k_{\text{else}} \sum_{p=1, p\neq i}^{N_t} H_{ij,z}^{p}. \tag{19}$$

For single-turn coils, $H_{ij,r}^{p}(p \neq i) = H_{ij,z}^{p}(p \neq i) = 0$, and thus the modification is not required. According to (14), the field strength at (ρ, θ) of the cross section is $I\rho/2\pi r_c^2$. Hence, the average squared field strength of the cross section becomes

$$\begin{aligned} H_{avg}^2 &= H_{\text{avg\_self}}^2 \\ &= \frac{1}{\pi r_c^2} \int_0^{2\pi} \int_0^{rc} \left(\frac{I\rho}{2\pi r_c^2}\right)^2 \rho d\rho d\theta \\ &= \frac{I^2}{8\pi^2 r_c^2}. \end{aligned} \tag{20}$$

The proximity-effect resistance of a single-turn coil can be expressed according to (3) and (20) as follows:

$$R_{\text{prox}} = \frac{n_0 \mu^2 \sigma r_s^4 r_i \omega^2}{16 r_c^2}. \tag{21}$$

It should be noted that k_{else} is mainly determined by the type of Litz-wire which is almost irrelevant to the dimensions of coils or the current frequency. Similar study has been carried out in [4], while the detailed explanation is lacked in [4]. When the Litz-wire type for coil design is determined, only one test is needed to decide k_{else} before coil design. Section II-B3 gives the method of determining k_{else}.

2) Modification Calculation Method of Conductive Resistance: According to (14), the field strength over the cross section of a single-turn coil is non-uniformly distributed. The strands of a perfect twisted Litz-wire can occupy the space uniformly in both radial and azimuthal directions, and thus the current flowing in all strands is uniform. However, most Litz-wires are twisted imperfectly, which can lead to an increase in conductive resistance as the current frequency increases [21]. A coefficient K_I is proposed in [21] to modify the conductive resistance as $K_I(\omega)R_{\text{cond}}$, and it has been found that K_I increases from 1 and then drops to 1 as frequency increase via simulation. However, the curve of K_I is irregular and distinguishing for different Litz-wires.

To address this problem, this article proposes a piecewise linear fitting method to estimate the conductive resistance versus frequency, which is denoted as $R_{\text{cond}}(\omega)$. A type of Litz-wire with 300 strands as an example is conducted. The radii of

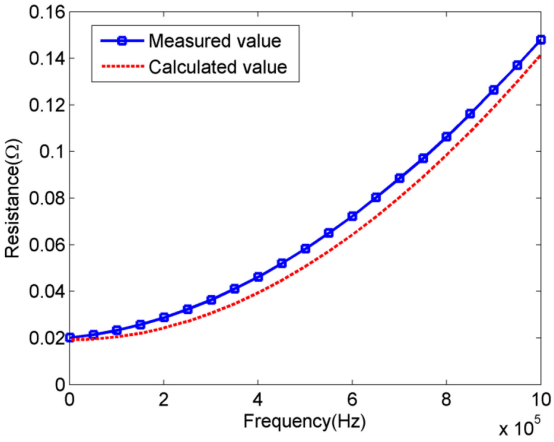

Fig. 7. Measured and calculated resistances of the single-turn coil versus frequencies.

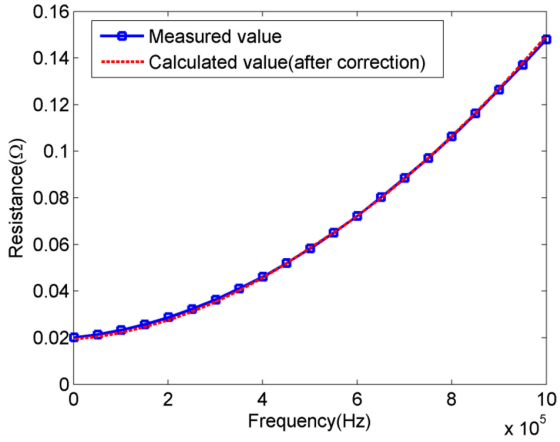

Fig. 8. Measured and calculated resistances of the single-turn coil versus frequencies after correction.

the Litz-wire and each strand are 1.12 and 0.05 mm, respectively. Then a single-turn coil is wound and its perimeter is 2.36 m. The skin effect can be approximately ignored when $r_s < \rho_{\text{skin}}$, and thus the range of experimental frequency is set to be between 1 kHz and 1 MHz, and 201 sample points ω_i (for $i = 1, 2, \ldots, 201$) are chosen uniformly. The resistances of the single-turn coil of ω_i (for $i = 1, 2, \ldots, 201$) are measured by impedance analyzer and calculated by (2) and (21). The result is compared in Fig. 7.

As shown in Fig. 7, there is an obvious difference between the measured value and calculated value. The error mainly is caused by the conductive resistance which is calculated via (2). In addition, the error increases first and then becomes small, which is consistent with the finding in [21]. Assuming that the error reaches its maximum value at ω_s and equals to $k_c \cdot R_{cond}$, then the linear fitting function of $R_{\text{cond}}(\omega)$ can be written as follows:

$$R_{\text{cond}}(\omega) = R_{\text{cond}}(1 + k_c \cdot \omega/\omega_s) \ (\omega \le \omega_s). \tag{22}$$

Though $R_{\text{cond}}(\omega)$ begins to decrease when $\omega > \omega_s$, the reduction is relatively small as shown in Fig. 7. For simplicity, let

$$R_{\text{cond}}(\omega) = R_{\text{cond}}(1 + k_c)(\omega > \omega_s). \tag{23}$$

The parameter k_c and ω_s can be determined as follows. According to (23), the measured resistance should almost be in agreement with the calculated value beyond a certain frequency (ω_s), if $R_{\text{cond}}(\omega)$ is replaced by $R_{\text{cond}}(\omega)(1 + k_c)$ at all frequencies. Therefore, the task is to try different k_c and compare the measured resistance with $R_{\text{cond}}(\omega)(1 + k_c)$. Compared with the maximum error and the mean square error, the average relative error is more understandable due to the fact that it can better reflect the whole calculation accuracy at the given frequency region. Therefore, the average relative error is employed to analyze the calculated result and the measured result in the study. From calculated results, it can be found that the relative errors between the calculated value and measured value are less than 1%, and the average of relative errors is 0.37%, when $k_c = 0.4$ and frequencies are larger than 500 kHz. Thus, k_c and ω_s are determined as 0.4 and 500 kHz, respectively. The conductive resistance can be calculated by (16) and (17), and the result is shown in Fig. 8. The average of relative errors between the calculated result and measured result for all frequency samples is calculated as 1.6%.

Furthermore, the coils with multiple turns are analyzed. Taking the *i*th turn of a multiple-turn coil as one example, if the field strength generated by other turns is stronger than that generated by the *i*th turn itself, the field strength distribution over the cross section will change dramatically from the original distribution expressed by (14). Hence, the superposed field strength created by all turns will be more uniform than the single-turn case. An index $\bar{\rho}$ is proposed to decide whether to use (2) to calculate conductive resistance and can be expressed as follows:

$$\bar{\rho} = \frac{\sum_{i=1}^{N_t} H^2_{\text{avg\_else}}(i)}{N_t} / H^2_{\text{avg\_self}}. \tag{24}$$

It should be noted that $H^2_{\text{avg\_else}}(i)$ is calculated with the correction coefficient k_{else}. As (24) shows, the index $\bar{\rho}$ indicates the contrast between the field strength generated by the *i*th turn and the rest of the turns. The Litz-wire with 300 strands is studied in this article. The result is that when $\bar{\rho} \le 1.32$, the conductive resistance should be calculated by (22) and (23); otherwise formula (2) should be used. $H^2_{\text{avg\_else}}(i)$ of coils wound closely is usually bigger than coils wound sparsely, and thus $\bar{\rho}$ of coils wound closely is higher relatively. It should be noted that the threshold of $\bar{\rho}$ is approximately determined as 1.32 through several experimental tests, because the threshold is determined by the twisting structure of Litz-wire and it is hard to analyze the functional relationship between them.

3) Determination of k_{else} and Verification of the Complete Calculation Method of AC Resistance: A test coil is wound to determine the coefficient k_{else} proposed in Section II-B-1). According to the result of Section II-B-2), the test coil is wound closely to avoid the influence of changing conductive resistance. The 300-strand Litz-wire mentioned above is used. N_t, d, and r_{out} of the test coil are 9, 2.5 mm, and 7.6 cm, respectively. First, 201 frequency sample points are chosen uniformly from 1 kHz to 1 MHz, and the resistance at those frequencies is measured

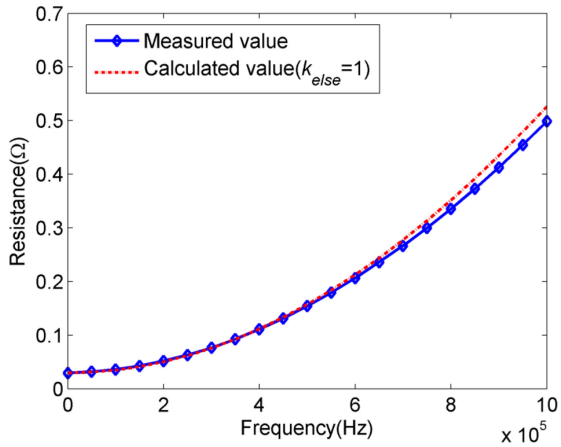

Fig. 9. Measured and calculated resistances of the test coil versus frequencies.

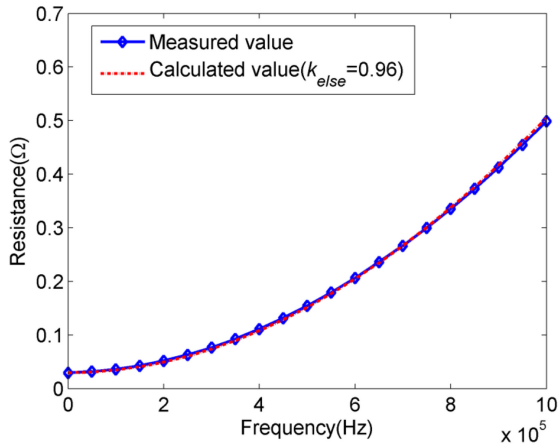

Fig. 10. Measured resistances and calculated resistances of the test coil versus frequencies after correction.

TABLE I
PARAMETERS OF EXPERIMENTAL COILS

Coil	N_t	r_{out}(cm)	d(mm)
A	12	11.65	2.5
B	8	7.90	2.5
C	8	8.75	5.0
D	8	9.00	6.0

by impedance analyzer. Then, let $k_{\text{else}} = 1$ and the resistance is calculated by (2) and (3). The result is shown in Fig. 9.

It can be observed from Fig. 9 that the calculated result is slightly larger than the measurement. Therefore, k_{else} decreases with an interval of 0.01. When k_{else} equals 0.96, the average of relative errors for all frequency samples is 1.0%. The modified result is given in Fig. 10. In addition, two or more test coil can be manufactured to make the modified result more precise.

Four experimental coils are manufactured to validate the complete ac resistance calculation method. The parameters of experimental coils are chosen randomly and listed in Table I.

The results are depicted in Fig. 11.

The average relative errors of the resistance for four coils are 2.6%, 2.5%, 2.1%, and 1.8%, respectively, which proves that the

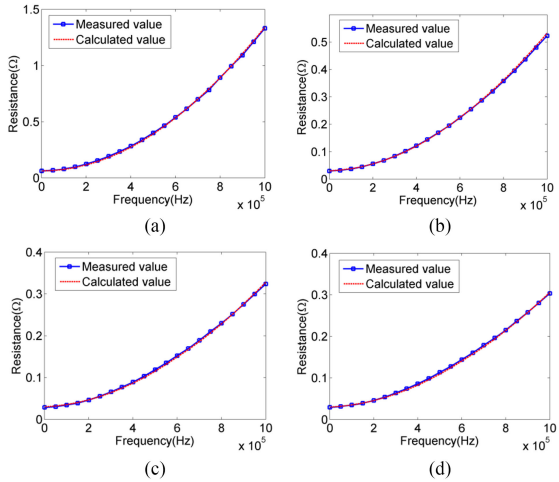

Fig. 11. Measured and calculated resistances versus frequencies for experimental coils. (a) Coil "A." (b) Coil "B." (c) Coil "C." (d) Coil "D."

TABLE II
MEASURED AND CALCULATED MUTUAL INDUCTANCE OF EXPERIMENTAL COILS

p_d(mm)	v(mm)	M_{mea}(μH)	M_{cal}(μH)	E_{re}
0	50	3.74	3.72	0.5%
0	75	2.37	2.32	2.1%
0	100	1.56	1.52	2.6%
17.5	50	3.62	3.56	1.7%

modified method can precisely predict the ac resistance of coils with various numbers of turns and turn-spacings. To compare the performance of the modified method to the original method, the ac resistance is also calculated with the original method in [20], in which (2) and (6) are applied to calculate conductive resistance and $H^2_{\text{avg}}(i)$, respectively. Consequently, the errors are 15.3%, 15.0%, 15.9%, and 17.1%, respectively. The large error is mainly caused by the conductive resistance (especially for coils wound sparsely) and the neglect of $H^2_{\text{cross}}(i)$. A coefficient λ is proposed and defined as $\sum_{i=1}^{N_t} [\text{H}^2_{\text{cross}}(i)/H^2_{\text{avg}}(i)]/N_t$ to estimate the overall proportion of $H^2_{\text{cross}}(i)$ in $H^2_{\text{avg}}(i)$. The value of λ is 13.1%, 12.6%, 5.6%, and 4.1%, respectively, for experimental coils. The results show that the term $H^2_{\text{cross}}(i)$ cannot be neglected for coils with large λ. The impact of resistance error on coil–coil efficiency will be discussed in Section III.

C. Calculation Method of Mutual Inductance

Using [22] and [23], the mutual inductance of two parallel coils can be calculated as follows:

$$M = \mu_0 \pi \int_0^{\infty} \sum_{i=1}^{N_t} \sum_{j=1}^{N_t} r_i r_j e^{-\beta v} J_1(\beta r_i) \times J_1(\beta r_j) J_0(\beta p_d) d\beta \tag{25}$$

where p_d denotes the distance between the axis of two coils.

For validation, coils with eight turns are wound to estimate the calculation formula. The measured and calculated results with various p_d and v are listed in Table II, in which M_{mea} and M_{cal} are, respectively, the measured mutual inductance and the calculated mutual inductance, and E_{re} is the relative error.

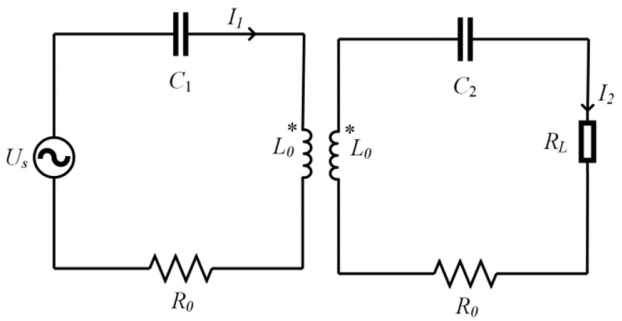

Fig. 12. S-S compensation topology of WPT systems.

It can be seen that all the relative error is less than 3.0%. The error may come from measurement due to the non-ideal measuring environment.

III. Efficiency Analysis and PSO-Based Coil Design Method

A. Efficiency Analysis Under S-S Compensation Topology and Corresponding Optimization Problem

Fig. 12 shows S-S compensation topology of WPT systems. U_s is the rms amplitudes of input voltage. I_1, I_2, C_1, and C_2 are respectively the current and the resonant capacitances of the primary side and the secondary side. L_0 is the self-inductance of coupling coils. R_0 and R_L are the total resistance of coil and circuit connection wires and the load resistance, respectively. For the S-S network, there is no reflected reactance and the reactance is independent of the load. In addition, less copper mass is required [15].

The secondary side is set to be complete resonant, while the primary side is set to be inductive to achieve the soft switching. The output power of load resistance and coil–coil efficiency of S-S topology can be written by

$$P_{\text{out}} = \frac{U_S^2 R_L (\omega M)^2}{\left[(\omega M)^2 + R_0(R_0+R_L)\right]^2 + X_1^2 (R_0+R_L)^2} \tag{26}$$

$$\eta_{\text{coil–coil}} = \frac{R_L}{R_L + R_0 + R_0 \frac{(R_0+R_L)^2}{(M\omega)^2}} \tag{27}$$

where ω, M, and X_1 are the working frequency, mutual inductance, and reactance of the primary side, respectively.

Defining the error of R_0 as ΔR_0, the error of coil–coil efficiency can be given by

$$\begin{aligned}\frac{\Delta\eta}{\eta} &= \frac{\eta(R_0) - \eta(R_0+\Delta R_0)}{\eta(R_0)} = 1 - \frac{\eta(R_0+\Delta R_0)}{\eta(R_0)} \\ &\approx \frac{\Delta R_0}{R_0}\left(\frac{1}{1+\Delta R_0/R_0 + (M\omega)^2/(R_L(R_L+R_0))}\right).\end{aligned} \tag{28}$$

The equation above can be used to evaluate the relative error of coil–coil efficiency caused by resistance calculation.

The coil–coil efficiency is determined by ω, R_L, and parameters of coil, as is shown in (21). Thus, the design problem can be expressed as follows:

$$\begin{cases} \max_{d,N_t,r_{\text{out}},\omega} \eta(d, N_t, r_{\text{out}}, \omega) \\ r_{\text{out}} \le r_{\text{out max}} \\ \omega_{\text{low}} < \omega < \omega_{\text{high}} \end{cases} \tag{29}$$

where $(\omega_{\text{low}}, \omega_{\text{high}})$ are the frequency design scope. Furthermore, for certain geometric parameters, there exists optimum working frequency corresponding to maximum efficiency [4], [18]. Supposing that the function between geometric parameters and optimum frequency is $\omega_{\text{opt}}(d, N_t, r_{\text{out}}) = g(d, N_t, r_{\text{out}})$, and ω_{opt} satisfies

$$\begin{aligned}&\text{for any fixed } (d, N_t, r_{\text{out}}): \\ &\eta(d, N_t, r_{\text{out}}, \omega_{\text{opt}}) = \eta(d, N_t, r_{\text{out}}, g(d, N_t, r_{\text{out}})) \\ &\ge \eta(d, N_t, r_{\text{out}}, \omega), \text{ for any } \omega \text{ in } (\omega_{\text{low}}, \omega_{\text{high}}).\end{aligned} \tag{30}$$

Assuming that the global optimum design parameter is $(d_{-glo}, N_{t-glo}, r_{\text{out}-glo}, \omega_{-glo})$ for the given design constraints, which satisfies $\eta(d_{-glo}, N_{t-glo}, r_{\text{out}-glo}, \omega_{-glo}) \ge \eta(d, N_t, r_{\text{out}}, \omega)$ for any d, N_t, r_{out}, ω. Then let (d, N_t, r_{out}) in (24) be $(d_{-glo}, N_{t-glo}, r_{\text{out}-glo})$, one can get $\eta(d_{-glo}, N_{t-glo}, r_{\text{out}-glo}, \omega_{\text{opt}}) \ge \eta(d_{-glo}, N_{t-glo}, r_{\text{out}-glo}, \omega)$ for any ω, and thus $\eta(d_{-glo}, N_{t-glo}, r_{\text{out}-glo}, \omega_{\text{opt}}) \ge \eta(d_{-glo}, N_{t-glo}, r_{\text{out}-glo}, \omega_{-glo})$. Since $(d_{-glo}, N_{t-glo}, r_{\text{out}-glo}, \omega_{-glo})$ is the global optimum solution, one can get $\omega_{-glo} = \omega_{\text{opt}}$. The proved conclusion shows that the optimum ω can be uniquely determined by the geometric parameters of the coil. Therefore, the optimization function can be written as $f_{\text{obj}} = \eta(d, N_t, r_{\text{out}}, \omega_{\text{opt}}) = \eta(d, N_t, r_{\text{out}}, g(d, N_t, r_{\text{out}})) = \eta_1(d, N_t, r_{\text{out}})$, and the optimization problem is as follows:

$$\begin{cases} \max_{d,N_t,r_{\text{out}}} \eta_1(d, N_t, r_{\text{out}}) \\ r_{\text{out}} \le r_{\text{out max}}. \end{cases} \tag{31}$$

The following part is to solve $g(d, N_t, r_{\text{out}})$. Using (3), one can obtain the following:

$$\begin{aligned}R_0 &= R_{\text{cond}} + R_{\text{prox}} \\ &\approx R_{\text{cond}} + \omega^2 \frac{n_0 \pi^2 \mu^2 \sigma r_s^4}{2I} \sum_{i=1}^{N_t} r_i H_{\text{avg}}^2(i) \\ &= R_{\text{cond}} + A\omega^2\end{aligned} \tag{32}$$

where A is the part unrelated to frequency. The denominator of (27) can be rewritten as follows:

$$\begin{aligned}f(\omega) = &\left(R_L + R_{\text{cond}} + A\omega^2\right) \\ &\cdot \left[1 + \left(\frac{R_{\text{cond}}}{(M\omega)^2} + \frac{A}{M^2}\right)\left(R_L + R_{\text{cond}} + A\omega^2\right)\right].\end{aligned} \tag{33}$$

Thus, maximizing the efficiency can be achieved by minimizing $f(\omega)$. Taking the derivative of $f(\omega)$ with respect to ω, it

yields

$$2A\omega + 4A\omega\left(\frac{R_{\rm cond}}{(M\omega)^2} + \frac{A}{M^2}\right)(R_L + R_{\rm cond} + A\omega^2) - \frac{2R_{\rm cond}}{M^2\omega^3}(R_L + R_{\rm cond} + A\omega^2)^2 = 0. \quad (34)$$

Let $x = A\omega^2$, and the equation above becomes

$$4x^3 + \left(\frac{2M^2}{A} + 6R_{\rm cond} + 4R_L\right)x^2 - (2R_{\rm cond}R_L^2 + 2R_{\rm cond}^3 + 4R_LR_{\rm cond}^2) = 0. \quad (35)$$

Denote (35) as $p(x) = 0$. The polynomial coefficients of $p(x)$ are $a = 4$, $b = 2M^2/A + 6R_{\rm cond} + 4R_L$, $c = 0$ and $d = -(2R_{\rm cond}R_L^2 + 2R_{\rm cond}^3 + 4R_LR_{\rm cond}^2$. Those coefficients are only decided by geometric parameters of coils. According to Cardano's formula of cubic equation, the discriminant of $p(x)$ is $\Delta = \frac{d}{27a^2}(\frac{b^3}{a^2} + \frac{27}{4}d)$. Due to the fact that $\frac{b^3}{a^2} \geq 4R_L^3 \gg 2(R_{\rm cond}R_L + R_{\rm cond}^3 + 2R_LR_{\rm cond}^2)$, it results $\Delta < 0$. Therefore, there are three real solutions for (35). The solutions are denoted as x_1, x_2, and x_3 ascending, then $g(x)$ achieves local minimum value at x_1 and x_3. According to Cardano's formula

$$\left(x_1 + \frac{a}{3b}\right) + \left(x_2 + \frac{a}{3b}\right) + \left(x_3 + \frac{a}{3b}\right) = 0. \quad (36)$$

Therefore $x_1 < 0$ and the optimal frequency $\omega_{\rm opt} = \sqrt{x_3/A}$.

The results are obtained based on the hypothesis that $R_{\rm cond}$ is constant for various frequencies. If $R_{\rm cond}$ is calculated by (22) and (23), approximate optimal frequency $\omega'_{\rm opt}$ can be obtained as above, and then the true optimal frequency can be found around $\omega'_{\rm opt}$ by PSO. Considering that the design scope of frequency is $(\omega_{\rm low}, \omega_{\rm high})$, then

$$\omega_{\rm opt} = \begin{cases} \sqrt{x_3/A} & (\omega_{\rm low} \leq \sqrt{x_3/A} \leq \omega_{\rm high}) \\ f^{-1}(\min(f(\omega_{\rm low}), f(\omega_{\rm high})))(\omega_{\rm high} \leq \sqrt{x_3/A}) \\ \omega_{\rm low}(\sqrt{x_3/A} \leq \omega_{\rm low}) \end{cases} = g(d, N_t, r_{\rm out}). \quad (37)$$

Three-objective (d, N_t, and $r_{\rm out}$) PSO algorithm is utilized to solve (31). The output of the algorithm is the optimal combination of (d, N_t, $r_{\rm out}$, ω), then U_s is determined by (26). The following section gives the steps of the PSO-based design method and one design example.

B. PSO-Based Coil Design Method

PSO algorithm is a kind of evolutionary algorithm. Particles of the swarm are moving to the optimal position iteratively through information sharing and position updating. There are several advantages of the PSO algorithm, such as easy to implement, fast convergence, and high accuracy [24], [25]. This article uses the conventional PSO algorithm to solve (31), and it is constructed as follows.

Step 1: Determine the number of particles (N), maximum generation (T), and initial parameters of each particle, such as (d^1, N_t^1, $r_{\rm out}^1$), (d^2, N_t^2, $r_{\rm out}^2$), …, (d^N, N_t^N, $r_{\rm out}^N$). Defining a storage matrix as

$$\text{pop} = \begin{pmatrix} d^1 & d^2 & \cdots & d^N \\ N_t^1 & N_t^2 & \cdots & N_t^N \\ r_{\rm out}^1 & r_{\rm out}^2 & \cdots & r_{\rm out}^N \end{pmatrix}.$$

Step 2: The update equation of the ith particle is

$$\text{pop}_{t+1}(j,i) = \text{pop}_t(j,i) + v_{t+1}(j,i)(\text{for } j = 1,2,3) \quad (38)$$

where t is the generation times, and $v_{t+1}(j,i)$ is the changing rate of the jth parameter of the ith particle, which is called velocity in the PSO algorithm. The velocity of each parameter can be expressed as follows:

$$v_{t+1}(1,i) = \alpha v_t(1,i) + c_1r_1(p\text{best}_t(1,i) - \text{pop}_t(1,i)) + c_2r_2(g\text{best}_t(1) - \text{pop}_t(1,i)) \quad (39)$$

$$v_{t+1}(2,i) = \text{round}(\alpha v_t(2,i) + c_1r_3(p\text{best}_t(2,i) - \text{pop}_t(2,i)) + c_2r_4(g\text{best}_t(2) - \text{pop}_t(2,i))) \quad (40)$$

$$v_{t+1}(3,i) = \alpha v_t(3,i) + c_1r_5(p\text{best}_t(3,i) - \text{pop}_t(3,i)) + c_2r_6(g\text{best}_t(3) - \text{pop}_t(3,i)) \quad (41)$$

where α is the inertia weight parameter, c_1 and c_2 are acceleration constants, r_i (for $i = 1, 2, \ldots, 6$) are random numbers uniformly distributed in the range of 0 and 1. $P\text{best}_t(j,i)$ (for $j = 1, 2, 3$) denotes the best position of the ith particle corresponding to maximum fitness value (η) up to current generation. $g\text{best}_t(j)$ (for $j = 1, 2, 3$) denotes the global best position of all particles up to current generation. In addition, α, c_1, and c_2 should satisfy (42) to guarantee the global convergence [26]

$$\begin{aligned} &0 \leq \alpha < 1; c_1 + c_2 > 0 \\ &0 < 1 - (\psi^2 + K - \alpha) + \alpha(\psi^2 - K - \alpha) - \alpha^3 \\ &< \frac{c_2^2(1+\alpha)}{6} \end{aligned} \quad (42)$$

where $\Psi = 1 + \alpha - (c_1 + c_2)/2$ and $K = (c_1^2 + c_2^2)/12$. Therefore α, c_1, and c_2 are denoted as 1/2, 2, and 2, respectively. The complete design procedures are given in Fig. 13.

A design example is given to explain the method, and the design constraints are as follows:

1) $P_{\rm out} = 20$ W;
2) $R_L = 2\ \Omega$;
3) $v = 7.5$ cm;
4) $r_{\rm outmax} = 100$ mm;
5) the total length of circuit connection wire is 0.6 m for both two sides;
6) the transmitting coil and receiving coil are designed to be identical and placed in coaxial.

In addition, due to the restriction of the practical design, the frequency design range is set to be 150 kHz $< f <$ 250 kHz. It should be noted that the design method is also appropriate for the other frequency region.

First, I_2 can be calculated as $\sqrt{10}$ A according to $P_{\rm out}$ and R_L. The current capacity of the 300-strand Litz-wire mentioned

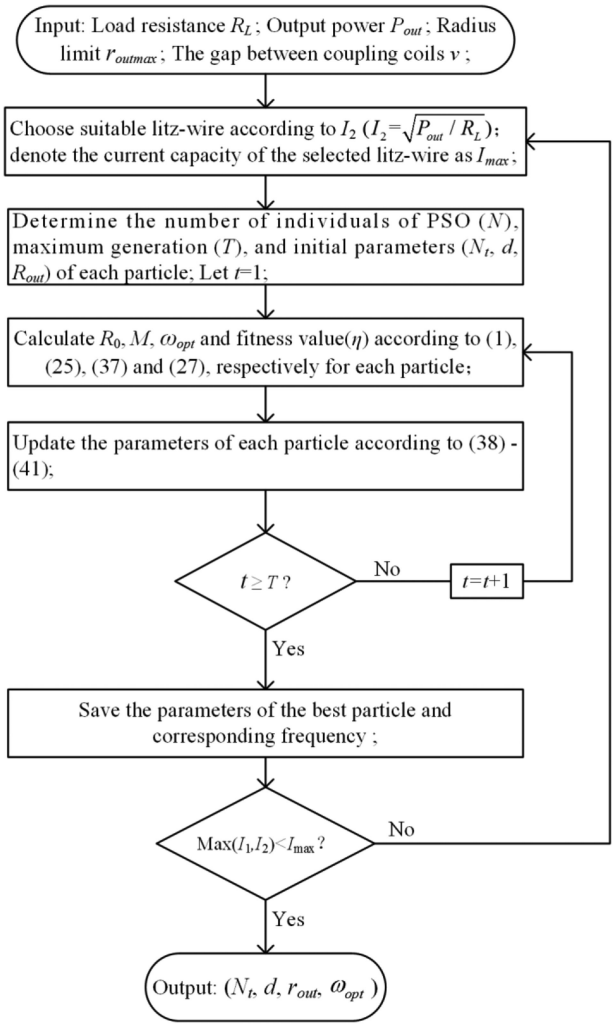

Fig. 13. Flowchart of the PSO-based design method.

TABLE III
OPTIMIZATION RESULTS OF THE DESIGN EXAMPLE

N	T	N_t	d	r_{out}
5	30	8	5.3mm	100mm
ω_{opt}	η	I_1	I_2	
194kHz	96.4%	1.90A	3.16A	

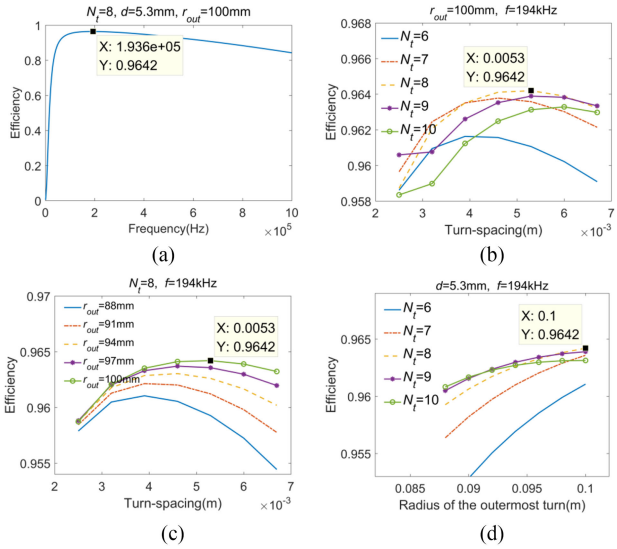

Fig. 14. Calculated coil–coil efficiency versus various parameters. (a) Coil–coil efficiencies versus frequencies when d, N_t, and $r_{\rm out}$ are fixed as 5.3, 8, and 100 mm, respectively. (b) Coil–coil efficiencies versus N_t and d when $r_{\rm out}$ and frequency are fixed as 100 mm and 194 kHz. (c) Coil–coil efficiencies versus d and $r_{\rm out}$ when N_t and frequency are fixed as 8 and 194 kHz. (d) Coil–coil efficiency versus N_t and $r_{\rm out}$ when d and frequency are fixed as 5.3 mm and 194 kHz.

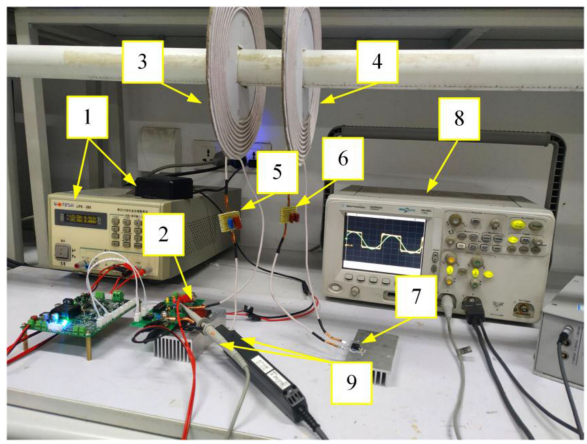

Fig. 15. Experimental prototype of the WPT system.

above is 7 A, and thus it can be used for the design. The algorithm is programmed with MATLAB and the optimization result is listed in Table III. The time cost is about 15 h, which is implemented by the computer (Intel Core i5-7500: 3.40 GHz, RAM: 8 GB). As shown in Table III, the maximum coil–coil efficiency can achieve 96.4% for the case of $N_t = 8, d = 5.3$ mm, $r_{\rm out} = 100$ mm, and $\omega = 194$ kHz.

Fig. 14(a) depicts the calculated coil–coil efficiency versus frequencies with fixed coil parameters. It can be seen that the optimal frequency exists around 193.8 kHz, which is in agreement with the $\omega_{\rm opt}$ obtained by (37). The relationship between the coil–coil efficiency and the coil parameters are further investigated, as is shown in Fig. 14(b)–(d). Taking into account readability, two-dimensional plots are used instead of three-dimensional plots. Fig. 14(b) plots the calculated coil–coil efficiency versus N_t and d when $r_{\rm out}$ and the working frequency are fixed as 100 mm and 194 kHz, respectively. It shows that the optimal combination of N_t and d is existed near (8, 5.3 mm). Moreover, Fig. 14(c) and (d) depict coil–coil efficiencies versus (d, $r_{\rm out}$) and (N_t, $r_{\rm out}$), respectively, and the results are consistent with the optimal design parameters shown in Table III.

IV. EXPERIMENTAL VALIDATION AND DISCUSSION

To validate the theoretical optimization result of the design example in Section III, an experimental prototype is established in Fig. 15. The prototype is mainly composed of nine parts: dc voltage sources, half-bridge inverter, transmitting coil, receiving coil, capacitance of the primary side, capacitance of the

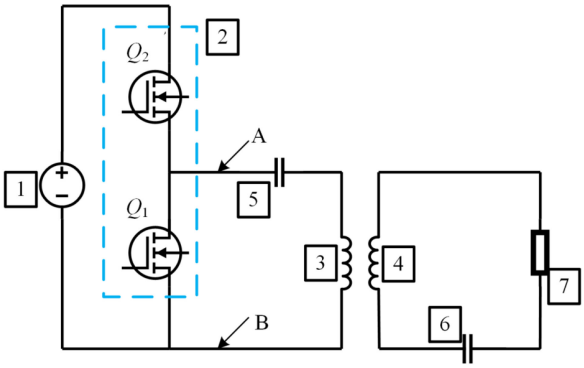

Fig. 16. Experimental prototype of the WPT system.

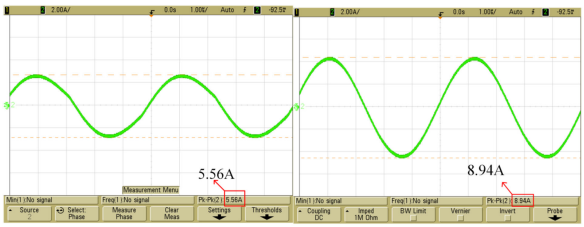

Fig. 17. (a) Current waveforms of the primary side. (b) Current waveforms of the secondary side.

secondary side, non-inductance load resistor, oscilloscope, and voltage/current probes. These parts are numbered from 1 to 9 in order, as shown in Fig. 15. The circuits diagram is illustrated in Fig. 16, point A and point B are the detect positions of voltage probes.

The transmitting coil and receiving coil are wound according to parameters in Table III. The measured resistance at 194 kHz is 54.2 mΩ while the calculated value is 54.7 mΩ, and thus the relative error is 1%. According to (28), the relative error of the coil–coil efficiency caused by resistance is 0.43%, which is relatively small. L_0 is measured as 15 μH, and thus $C_2 = 1/(L_0\omega^2) = 44.4$ nF. The impedance of the primary side needs to be inductive to achieve soft switching, and the appropriate impedance angle is 15°, that is based on (43), C_1 is calculated to be 48.5 nF

$$\frac{\omega L - 1/(\omega C_1)}{(\omega M)^2/(R_0 + R_L) + R_0} \approx \tan 15^\circ. \tag{43}$$

Fig. 17 shows the current waveforms of the primary side and secondary side, respectively. Fig. 18 depicts the current and voltage waveforms between notes A and B in Fig. 16, and the impedance angle can be calculated as follows: $\theta = 220/(10^9/194\,000) \cdot 360^\circ \approx 15.4^\circ$.

The output and input power can be obtained as 19.98 and 20.9 W according to the amplitudes of the current and voltage waveforms. Thus, the coil–coil efficiency is 95.6%. The experimental coil–coil efficiency is only 0.8% lower than the theoretical value. The error may come from misalignment of complete resonance in secondary side and joint loss.

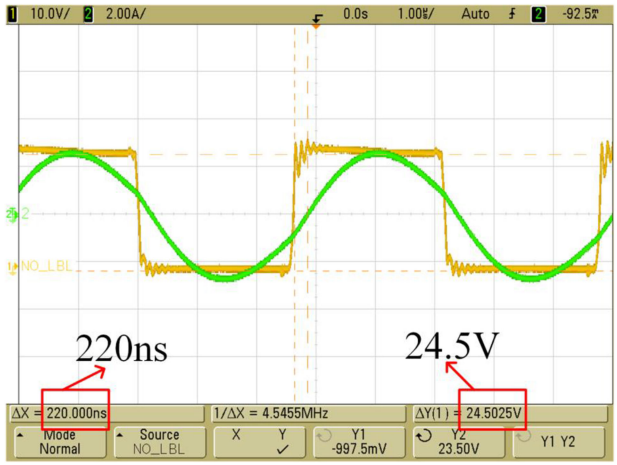

Fig. 18. Current and voltage waveforms of the primary side.

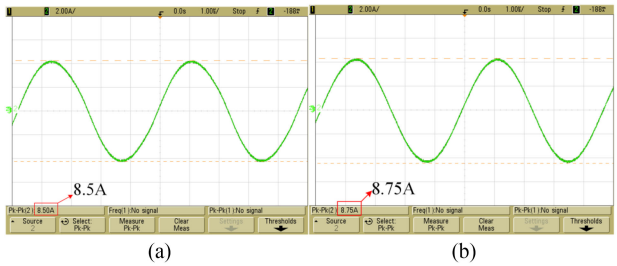

Fig. 19. (a) Current waveforms of the primary side. (b) Current waveforms of the secondary side.

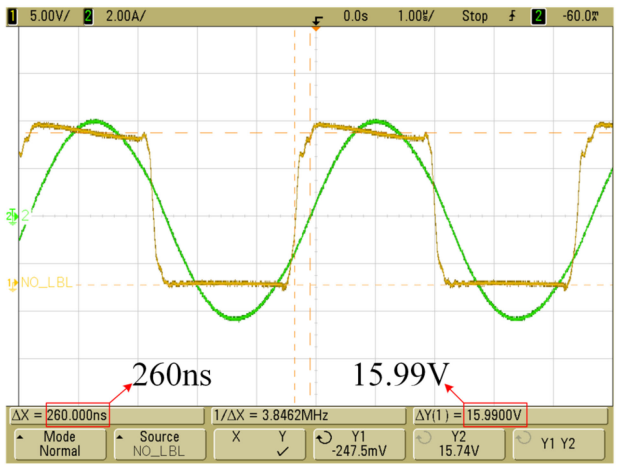

Fig. 20. Current and voltage waveforms of the primary side.

As a contrast, the method proposed in [8] is also applied to solve the design example of this article. The results of the contrast method are: $r_{\text{out}} = 100$ mm, $d = 8.3$ mm, $N_t = 6.3$, and $\omega = 211$ kHz. Due to the fact that the calculated coil–coil efficiencies of $N_t = 6$ and $N_t = 7$ are 94.3% and 95.9%, respectively, N_t is chosen to be 7, and another experiment is conducted based on those design parameters. The waveforms of currents and voltages are shown in Figs. 19 and 20, and it shows that the experimental coil–coil efficiency of the comparable method is

94.0%, which is lower than that of the PSO-based method. Compared to the conventional method, the calculation formulas of ac resistance and inductance of the PSO-based method are more accurate. In addition, the design parameters can move closer to the global optimal solution with the PSO-based method.

V. Conclusion

A PSO-based method is proposed to design the coupling coil for WPT systems with special constraints. The innovation is that the ac resistance and the mutual inductance of coils are calculated by the precise analytical method, and thus FEA software is not required anymore, which means the design process can be automatic and faster. The modified calculation method of ac resistance is universal for spiral coils wound closely or sparsely, and the average relative errors between the calculated values and experimental values are less than 3.0% for all experimental coils. A design example is given to validate the design method, and a 20-W WPT prototype is built. The coil–coil efficiencies of optimization results and experimental results are 96.4% and 95.6% respectively, which shows the precision of the design method. Moreover, a conventional method is applied to solve the design example for comparison, and experimental results show that its coil–coil efficiency is 94.0%, which is lower than 95.6%. Though only S-S compensation network is studied in this article, the PSO-based design method can be utilized in other compensation topologies. The limitation of this article is that only the coupling coils without magnetic core is studied. The complex case with magnetic core will be studied in the future.

References

[1] S. Moon and G. Moon, "Wireless power transfer system with an asymmetric four-coil resonator for electric vehicle battery chargers," *IEEE Trans. Power Electron.*, vol. 31, no. 10, pp. 6844–6854, Oct. 2016.

[2] C. Xiao, K. Wei, D. Cheng, and Y. Liu, "Wireless charging system considering eddy current in cardiac pacemaker shell: Theoretical modelling, experiments, and safety simulations," *IEEE Trans. Ind. Electron.*, vol. 64, no. 5, pp. 3978–3988, May 2017.

[3] X. Li, C. Tang, X. Dai, P. Deng, and Y. Su, "An inductive and capacitive combined parallel transmission of power and data for wireless power transfer systems," *IEEE Trans. Power Electron.*, vol. 33, no. 6, pp. 4980–4991, Jun. 2018.

[4] Q. Deng *et al.*, "Frequency-dependent resistance of Litz-wire square solenoid coils and quality factor optimization for wireless power transfer," *IEEE Trans. Ind. Electron.*, vol. 63, no. 5, pp. 2825–2837, May 2016.

[5] J. P. K. Sampath, A. Alphones, and H. Shimasaki, "Coil design guidelines for high efficiency of wireless power transfer (WPT)," in *Proc. IEEE Region 10 Conf.*, Feb. 2016, pp. 726–729.

[6] J. Cho, J. Sun, H. Kim, J. Fan, Y. Lu, and S. Pan, "Coil design for 100 kHz and 6.78 MHz WPT system: Litz and solid wires and winding methods," in *Proc. IEEE Int. Symp. Electromagn. Compat. Signal/Power Integrity*, Aug. 2017, pp. 803–806.

[7] S. Valtchev, B. Beatriz, K. Brandisky, and J. B. Klaassens, "Resonant contactless energy transfer with improved efficiency," *IEEE Trans. Power Electron.*, vol. 24, no. 3, pp. 685–699, Mar. 2009.

[8] R. Tanzania, F. H. Choo, and L. Siek, "Design of WPT coils to minimize AC resistance and capacitor stress applied to SS-topology," in *Proc. 41st Annu. Conf. IEEE Ind. Electron. Soc.*, Nov. 2015, pp. 118–122.

[9] T. Noda, T. Nagashima, and H. Sekiya, "A design of inductively coupled wireless power transfer system with coupling coil optimization," in *Proc. IEEE Int. Telecommun. Energy Conf.*, Oct. 2015, pp. 1–6.

[10] A. A. S. Mohamd, S. An, and O. Mohammed, "Coil design optimization of power pad in IPT system for electric vehicle applications," *IEEE Trans. Magn.*, vol. 54, no. 4, Apr. 2018, Art. no. 9300405.

[11] T. H. High, G. H. Yun, and W. Y. Lee, "High Q-factor compact coils having non-uniform wire width for wireless power transfer system," in *Proc. URSI Asia-Pac. Radio Sci. Conf.*, Aug. 2016, pp. 854–657.

[12] H. Kim *et al.*, "Coil design and measurements of automotive magnetic resonant wireless charging system for high-efficiency and low magnetic field leakage," *IEEE. Trans. Microw. Theory Techn.*, vol. 64, no. 2, pp. 383–400, Feb. 2016.

[13] J. Sallan, J. L. Villa, A. Llombart, and J. F. Sanz, "Optimal design of ICPT systems applied to electric vehicle battery charge," *IEEE Trans. Ind. Electron.*, vol. 56, no. 6, pp. 2140–2149, Jun. 2009.

[14] A. Ibrahim and M. Kiani, "A figure-of-merit for design and optimization of inductive power transmission links for millimeter-sized biomedical implants," *IEEE Trans. Biomed. Circuits Syst.*, vol. 10, no. 6, pp. 1100–1111, Dec. 2016.

[15] M. Dehghanian, A. Namadmalan, and M. Saradarzadeh, "Optimum design for series-series compensated inductive power transfer systems," in *Proc. 8th Power Electron., Drive Syst. Technol. Conf.*, Feb. 2017, pp. 365–370.

[16] Y. Yao, Y. Wang, X. Liu, Y. Pei, D. Xu, and X. Liu, "Particle swarm optimization based on parameter design method for S/CLC compensated IPT systems featuring high tolerance to misalignment and load variation," *IEEE Trans. Power Electron.*, vol. 34, no. 6, pp. 5268–5282, Jun. 2019.

[17] J. Liu, Q. Deng, D. Czarkowski, M. K. Kazimierczuk, H. Zhou, and W. Hu, "Frequency optimization for inductive power transfer based on AC resistance evaluation in Litz-wire coil," *IEEE Trans. Power Electron.*, vol. 34, no. 3, pp. 2355–2363, Mar. 2019.

[18] I. Lope, J. Acero, and C. Carretero, "Analysis and optimization of the efficiency of induction heating applications with Litz-wire planar and solenoidal coils," *IEEE Trans. Power Electron.*, vol. 31, no. 7, pp. 5089–5101, Jul. 2014.

[19] Y. Suzuki, I. Hasegawa, S. Sakabe, and T. Yamada, "Effective electromagnetic field analysis using finite element method for high frequency transformers with Litz-wire," in *Proc. Int. Conf. Elect. Mach. Syst.*, Oct. 2008, pp. 4388–4393.

[20] J. Acero, R. Alonso, J. M. Burdo, L. A. Barragan, and D. puyal, "Frequency-dependent resistance in Litz-wire planar windings for domestic induction heating appliances," *IEEE Trans. Power Electron.*, vol. 21, no. 4, pp. 856–866, Jul. 2006.

[21] T. Guilod, J. Huber, F. Krismer, and J. W. Kolar, "Litz wire losses: Effects of twisting imperfections," in *Proc. IEEE 18th Workshop Control Model. Power Electron.*, Jul. 2017, pp. 1–8.

[22] W. G. Hurley and M. C. Duffy, "Calculation of self and mutual impedances in planar magnetic structures," *IEEE Trans. Magn.*, vol. 31, no. 4, pp. 2416–2422, Jul. 1995.

[23] J. Acero, C. Carretero, I. Lope, R. Alonso, Ó. Lucia, and J. M. Burdio, "Analysis of the mutual inductance of planar-lumped inductive power transfer systems," *IEEE Trans. Ind. Electron.*, vol. 60, no. 1, pp. 410–420, Jan. 2013.

[24] M. Clerc and J. Kennedy, "The particle swarm-explosion, stability, and convergence in a multidimensional complex space," *IEEE Trans. Ind. Electron.*, vol. 6, no. 1, pp. 58–73, Feb. 2002.

[25] J. H. Lee, J. Song, D. Kim, J. Kim, Y. Kim, and S. Jung, "Particle swarm optimization algorithm with intelligent particle number control for optimal design of electric machines," *IEEE Trans. Ind. Electron.*, vol. 65, no. 2, pp. 1791–1798, Feb. 2018.

[26] M. Jiang, Y. P. Luo, and S. Y. Yang, "Stochastic convergence analysis and parameter selection of the standard particle swarm optimization algorithm," *Inf. Process. Lett.*, vol. 102, no. 1, pp. 8–16, Apr. 2007.

Guo Wei received the M.Sc. degree in electrical engineering from the Harbin Institute of Technology (HIT), Harbin, China, in 1991, and the Ph.D. degree in electrical engineering from Saga University, Honjomachi, Japan, in 2003.

He is currently a Professor with the HIT. His main research interests include wireless power and information transfer, sensing technology, instrumentation and signal processing.

Xiulang Jin received the B.S. degree in mathematics and applied mathematics, and the M.E degree in instruments science and technology from the Harbin Institute of Technology (HIT), Harbin Institute of Technology (HIT), Harbin, China, in 2017 and 2019, respectively.

His research interests include wireless power transfer.

Chao Wang received the B.S. degree in measurement and control technology and instrument from Nanchang University, Nanchang, China, in 2014. He is currently working toward the Ph.D. degree in electrical engineering with the Harbin Institute of Technology, Harbin, China.

His research interests include wireless power transfer and dynamic wireless charging for electric vehicles.

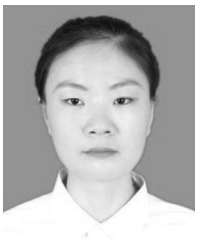

Jing Feng received the B.E. degree in electrical engineering and automation and the M.E degree in electronics and communication engineering from Henan Normal University, Henan, China, in 2015 and 2019, respectively. She is currently working toward the Ph.D. degree in electrical engineering with the School of Electrical engineering and Automation, Harbin Institute of Technology, Harbin, China.

Her research interests include wireless power transfer.

Chunbo Zhu was born in Harbin, China. He received the B.E., M.A., and Ph.D. degrees in electrical engineering from the Harbin Institute of Technology (HIT), Harbin, China, in 1987, 1992, and 2001, respectively.

Since 1987, he has been with the HIT, and is currently a Full Professor and a Lecturer with the Department of Automation Measurement and Control. From 2003 to 2004, he was a Senior Researcher with the Power Electric Center, National University of Ireland, Galway, Ireland. His current research interests include wireless power transmission, battery management systems, electric vehicles, and hybrid electric vehicles.

Milyaev Igor Matveevich's, photograph and biography not available at the time of publication.